HIGH TECHNOLOGY LETTERS | Vol. 30 No. 3 | Sep. 2024 | pp. 263-270

doi:10.3772/j.issn.1006-6748.2024.03.005

Research on heat dissipation characteristics of magnetic fluid bearings under multiple field coupling effects①

CHEN Liwen (陈丽文)②*, WU Weiying*, GAO Dianrong**, ZHAO Jianhua**, CUI Bingyan*

(* College of Mechanical Engineering, North China University of Science and Technology, Tangshan 063210, P. R. China)

(** College of Mechanical Engineering, Yanshan University, Qinhuangdao 066000, P. R. China)

Abstract

This paper analyzes the sources of heat losses in magnetic fluid bearings, proposes various coupling relationships of physical fields, divides the coupled heat transfer surfaces while ensuring the continuity of heat flux density, and analyzes the overall heat dissipation pathways of the bearings. By changing parameters such as input current, rotor speed, and inlet oil flow rate, the study applies a multi-physics field coupling method to investigate the influence of different parameters on the temperature field and heat dissipation patterns of the bearings, which is then validated through experiments. This research provides a theoretical basis for the optimal design of magnetic fluid bearing systems.

Key words: magnetic fluid bearing, multi-physics field coupling, multiple parameter variation, heat dissipation pattern

0 Introduction

The heat generated during the operation of magnetic fluid bearings causes a temperature increase in various parts of the main spindle, leading to thermal deformation and changes in the bearing clearance. Compared with traditional calculation methods, numerical methods with multi-physics field coupling provide more realistic results in the analysis of temperature rise[1-2]. Shi et al.[3] developed a thermal-structural coupling mathematical model for the permanent magnet synchronous motor electric spindle, highlighting the impact of axial temperature difference on machining accuracy. Yin et al.[4] used an indirect coupling method to establish a fluid-heat-conduction-solid coupling mathematical simulation model for liquid hydrostatic spindles, analyzing the effects of certain structural parameters and operating parameters on spindle temperature rise. Holkup et al.[5] established a thermal-solid coupling model for electric spindles, analyzing the temperature field and heat distribution caused by the motor and bearings; while other researchers used the computational fluid dynamics-fluid structure interaction (CFD-FSI) method to study fluid dynamic lubrication analysis and structural elastic deformation in rotor bearing systems based on the isothermal assumption[6-7].

This study conducts a multi-field coupling simulation analysis of the temperature field and heat dissipation patterns in magnetic fluid bearings, and further visually analyzes the temperature rise issue through experiments, providing a theoretical basis for the reasonable design of magnetic fluid bearing systems.

1 Magnetic fluid bearing system and coupling relationships

1.1 Magnetic fluid bearing system

The magnetic fluid bearing comprises two sets of bearing systems: electromagnetic suspension and liquid static pressure. The primary support is provided by electromagnetic suspension, with static pressure support as a secondary means, enabling dual support that can be adjusted in real-time. The magnetic fluid bearing system is depicted in Fig. 1.

The magnetic fluid bearing system mainly consists of components such as stator (made of silicon steel with chrome plating), rotor, magnetic sleeve (made of cold-rolled non-oriented silicon steel with chrome plating), coil, end cap, and seal cap. Inside the stator,

① Supported by the National Natural Science Foundation of China (No. 52075468), the Natural Science Foundation of Hebei Province (No. E2020203052), the Key Scientific Research Projects of North China University of Technology (No. ZD-YG-202306-23) and the Tangshan Science and Technology Project (No. 23130201E).

② To whom correspondence should be addressed. E-mail: chenliwen@ncst.edu.cn.

Received on Nov. 2, 2023

there are eight cylindrical magnetic pole structures evenly distributed in the circumferential direction. Coils are wound around the magnetic poles, generating electromagnetic force when powered. At the central position of the magnetic pole, there is an inlet for fluid. The oil is pumped out from the oil tank, and as it flows through the end face between the magnetic pole and the magnetic sleeve, it forms a static pressure supporting chamber. Under uninterrupted oil supply conditions, it creates a liquid static pressure supporting force[8].

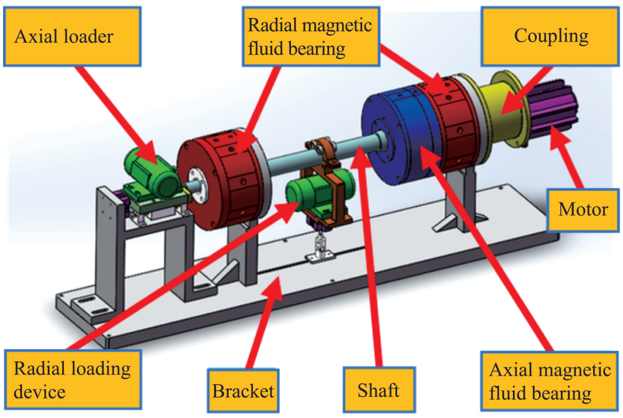

Fig. 1 Composition diagram of magnetic-liquid double suspension bearing system

1.2 The coupling relationship of magnetic fluid bearings

In magnetic fluid bearings, there are four physical fields: magnetic field, flow field, temperature field, and structural field, which interact with and influence each other, forming mutual coupling relationships. These coupling relationships are divided into four aspects.

(1) Fluid-thermal coupling: in the system, this is manifested as the interaction between the fluid field and the temperature field of magnetic liquid bearings. It leads to increased system losses, temperature rise, and an increase in the dynamic viscosity of the hydraulic oil provided by the bearing's static pressure system with increasing bearing temperature. It also results in an increasing in internal frictional forces due to the interaction of fluids[9].

(2) Fluid-structure thermal coupling, or conjugate heat transfer: when heat exchange occurs between the fluid and structure, the thermal boundary conditions (such as temperature and heat transfer coefficients) between them are calculated in real-time during the conjugate heat transfer process and cannot be preset. In the context of magnetic liquid bearings, this is observed in the heat transfer process between coils and fluid, as well as between the stator and the fluid[10].

(3) Structural-thermal coupling: this coupling relationship involves the interaction between the structural field of magnetic liquid bearings and the temperature field. It is manifested by the increase in temperature of the stator and rotor during the operation of the bearing, leading to thermal deformation in the overall radial bearing and its components[11].

(4) Electromagnetic-thermal coupling: this coupling relationship arises from the interaction between the magnetic field generated by the current passing through the magnetic liquid bearing and the temperature field. It is observed in the bearing as an increase in eddy current losses in the rotor due to changes in operational parameters, leading to thermal deformation of the rotor during operation[12].

2 Analysis of thermal losses in magnetic fluid bearings

The thermal losses of the bearing are mainly composed of two parts, namely, the thermal losses of the electromagnetic support system and the thermal losses of the hydrostatic support system.

2.1 Calculation of thermal losses in the electromagnetic support system

The thermal losses in electromagnetic bearings are generally composed of copper losses (heat generated due to coil resistance), iron losses (eddy current losses and hysteresis losses), and windage losses (air friction losses). In this research system, the stator remains stationary, and direct current is passed through the coils wound around the stator. Therefore, the stator does not produce iron losses, and the space between the stator and rotor is filled with hydraulic oil, eliminating windage losses. Therefore, it is only necessary to calculate the copper losses.

Refer to Eq. (1) for the calculation of coil copper losses.

$$P_{cu} = I^2 R = I^2 \rho L \tag{1}$$

where, P_{cu} is coil copper losses, W; I is current, A; R is wire resistance, Ω; L is wire length, m; ρ is wire resistivity, $\Omega \cdot m^{-1}$.

The heat generation rate of each coil is as shown in Eq. (2)[13].

$$q_{cu} = \frac{P_{cu}}{V_{cu}} = \frac{I^2 \rho L}{SL} = \frac{I^2 \rho}{S} \tag{2}$$

where, q_{cu} is heat generation rate of each coil, $W \cdot m^{-3}$; V_{cu} is coil volume, m^3; S is cross-sectional area of the wire, m^2.

2.2 Calculation of heating loss in liquid hydrostatic bearing systems

The heat loss in liquid hydrostatic bearings mainly comes from the power loss of the lubrication system and the fluid friction loss when there is relative motion between the fixed and rotating components. Magnetic fluid bearings are equipped with a cooling system, and the inlet oil temperature is considered constant, so the power loss of the lubrication system is not taken into account; only the fluid friction loss needs to be calculated.

The calculation of the frictional force in a support cavity is as shown in Eq. (3)[14].

$$F_{\mathrm{f}} = \frac{\eta_t v}{h_0} A_f \tag{3}$$

where, η_t is dimensionless fluid friction coefficient; v is sliding speed of the sliding component, $\mathrm{m \cdot s^{-1}}$; h_0 is oil film thickness, mm; A_f is effective frictional area of the support cavity, $\mathrm{mm^2}$. Then, the fluid friction loss can be calculated using Eq. (4).

$$N_f = F_f \cdot v = \eta_t v^2 \frac{A_f}{h_0} \tag{4}$$

2.3 Boundary conditions

The initial design parameters and material properties of the magnetic fluid bearings are shown in Tables 1 and 2.

Table 1 Initial design parameter

	Type	Density $P/(\mathrm{kg \cdot m^{-3}})$	Specific heat capacity $C/(\mathrm{J/kg/℃})$	Heat conductivity $K/(\mathrm{W/m/℃})$	Elasticity modulus E/MPa	Dilatation coefficient $\beta/(\mathrm{\mu m/℃})$
Stator	23QG385	7 650	502	16.27	1.95×10^5	11.2
Coil	Cu	8 978	381	387.60	1.10×10^5	18.5
Oil	LHM-46#	870	1 880	0.12	—	—

Table 2 Material properties

Input current i_0/A	Flow $q_0/(\mathrm{L \cdot min^{-1}})$	Rotate speed $n/(\mathrm{r \cdot min^{-1}})$	Oil temperature T/℃
2	0.02	2 000	20
Wire diameter D/mm	Wire resistivity $\rho_0/(\Omega \cdot \mathrm{m})$	Number of turns per coil N/dimensionless	Magnetic pole thickness A/mm
0.4	0.133	143	20
Magnetic pole axial length B/mm	Film thickness $h_0/\mathrm{\mu m}$	Oil viscosity(20 ℃) $\mu/(\mathrm{Pa \cdot s})$	
45	30	4.136×10^{-2}	

Using coupled heat transfer methods to solve the thermal exchange between the stator, coil, and fluid, ensuring the continuity of heat between the coupled surfaces. The boundary conditions for each heat transfer surface can be divided into the following three parts.

(1) Heat transfer coefficients between the two ends of the rotor and the external environment

When the rotor rotates, its two side faces are in relative motion with the air. The heat transfer coefficient can be calculated according to Eq. (5) for this phenomenon[15].

$$h_1 = 7.8 u^{0.78} = 7.8 \left(\frac{\pi r n}{40}\right)^{0.78} \tag{5}$$

where, h_1 is heat transfer coefficient between the two ends of the rotor and the external environment, $\mathrm{W/(m^2 \cdot ℃)}$; u is linear velocity of the rotating shaft surface, $\mathrm{m \cdot s^{-1}}$; r is length of the rotating radius, m; n is rotor speed, $\mathrm{r \cdot min^{-1}}$.

When the rotational speed is $n = 2\,000\ \mathrm{r \cdot min^{-1}}$, the heat transfer coefficient between the two ends of the rotor and the external environment is $h_1 = 25.12\ \mathrm{W/(m^2 \cdot ℃)}$.

(2) The heat dissipation rate of the stator casing

The heat transfer between the stator casing and the external environment includes two methods: natural convection and thermal radiation. According to Ref. [2], $h_2 = 9.7\ \mathrm{W/(m^2 \cdot ℃)}$.

(3) The heat transfer coefficient between the coupled heat transfer surfaces

Because the heat generation in the coil and the fluid cooling of the coil occur simultaneously, the heat transfer rate between them cannot be predetermined. In Fluent, the coupled heat transfer surfaces between fluid-coil, coil-stator magnetic poles, and stator-fluid are set as coupled heat transfer surfaces to ensure continuous heat flux density between the three.

The three heat transfer surfaces are shown in Fig. 2.

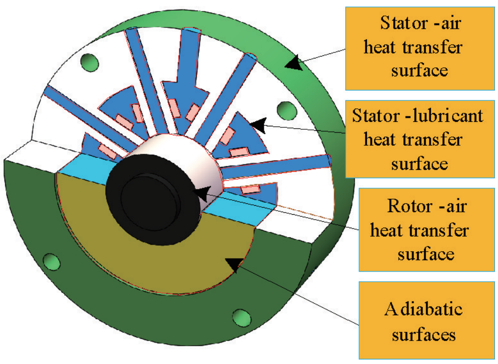

Fig. 2 Heat transfer surface of magnetic-liquid bearing

2.4 The overall heat transfer path of the bearing

The heat transfer path between the stator, winding coils, magnetic core, rotor shaft, and the surrounding air is shown in Fig. 3.

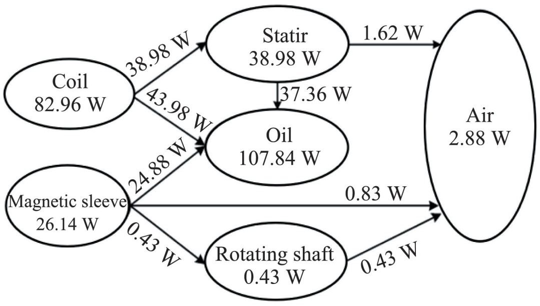

Fig. 3 Heat dissipation of bearing system

From Fig. 3, it can be observed that there are two ways for the heat dissipation of coil losses: one is through heat conduction to the stator, and the other is through convective heat transfer to the fluid. The magnetic core has three paths, adding additional heat dissipation routes: dissipating heat to the air through convective heat transfer. Analyzing the data in the figure, the total copper loss in the coil is 82.96 W, of which 38.98 W (46.99%) is transferred to the stator, and 43.98 W (53.01%) is carried away by the oil for absorption. The stator absorbs 37.36 W (95.84%) of the heat from the coil, with 1.62 W (4.16%) dissipating into the air. The eddy current loss in the magnetic core is 26.14 W, of which 24.88 W (95.18%) is absorbed by the oil, 0.83 W (3.18%) dissipates into the air, and 0.43 W (1.64%) is absorbed by the rotor shaft. In the end, all the heat of 109.10 W, 98.84% (107.84 W) is transferred to the oil, and 1.16% (2.88 W) is dissipated into the air. Therefore, it is evident that oil is the main cooling pathway for the bearing, and the cooling efficiency of the oil can reach 98.84%.

3 The impact of parameter changes on the heat dissipation patterns of bearings

The heat loss of the bearing has only two pathways, oil and the atmosphere. With changes in parameters, the heat dissipation characteristics of the bearing's coil and magnetic core will also change. By extracting the heat transfer rates between various coupled heat exchange surfaces, an analysis of the overall heat dissipation characteristics of the bearing is conducted, exploring how parameter changes influence the dissipation characteristics of the two major heat sources in the bearing.

3.1 The relationship between input current parameters

An increase in input current directly results in an increase in copper losses in the bearing coil and eddy current losses in the magnetic core, leading to an intensification of bearing temperature rise. The study of the dissipation characteristics of the two major heat sources in the bearing with the variation of input current is presented in Table 3.

Table 3 Change rule of heat transfer rate of bearing with input current

Input current I/A	Eddy current loss → fluid heat transfer rate P_1/W	Eddy current loss → atmospheric heat transfer rate P_2/W	Coil copper loss → fluid heat transfer rate P_3/W	Coil copper loss → atmospheric heat transfer rate P_4/W
2.0	24.88	1.26	81.36	1.62
2.2	30.48	1.55	98.44	1.96
2.4	36.33	1.86	117.15	2.34
2.6	43.60	2.20	137.50	2.73
2.8	50.80	2.58	159.47	3.17

With the increase in input current, the copper losses in the bearing coil and eddy current losses increase as well. As shown in Table 3, the heat transfer rates of eddy current losses and coil copper losses to the fluid and atmosphere increase with the increase in input current. The proportion of losses transferred to the atmosphere and fluid is analyzed, as illustrated in Fig. 4.

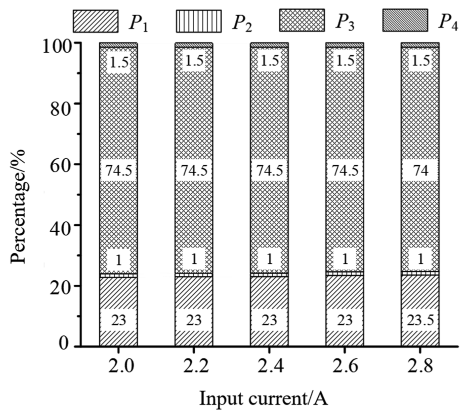

Fig. 4 Change rule of ratio of heat transfer rate with input current

3.2 The relationship between the rotor rotational speed and its parameters

Due to the synchronous rotation of the rotor shaft and the magnetic core, as the rotational speed increases, the relative velocity between the rotor end and the air increases. According to Eq. (5), it is evident that the heat transfer coefficient between the rotor and the air linearly increases with the rotational speed. This will inevitably lead to an increase in heat transfer from the magnetic core to the atmosphere, subsequently affecting the heat dissipation pattern of the magnetic core. However, the rotation of the rotor does not affect coil losses, nor does it impact the heat dissipation pattern of coil losses. The heat dissipation pattern of the bearing with respect to rotor rotational speed variation is presented in Table 4.

Table 4 Change rule of heat transfer rate of bearing with revolution speed

Rotate speed n/r · min^{-1}	Eddy current loss → fluid heat transfer rate P_1/W	Eddy current loss → atmospheric heat transfer rate P_2/W	Coil copper loss → fluid heat transfer rate P_3/W	Coil copper loss → atmospheric heat transfer rate P_4/W
2 000	24.88	1.26	81.36	1.62
3 000	40.17	2.74	81.35	1.62
4 000	53.84	4.54	81.35	1.63
5 000	67.64	6.70	81.34	1.63
6 000	80.68	9.13	81.33	1.64

According to Table 4, it can be observed that the heat dissipation pattern of the bearing's coil copper losses remains unchanged with an increase in rotor rotational speed. The heat transfer rate of eddy current losses to the atmosphere and fluid increases, while the heat transfer rate of coil copper losses to the fluid and atmosphere remains relatively constant. The changes in the proportion between P_1 and P_4 are analyzed, as shown in Fig. 5.

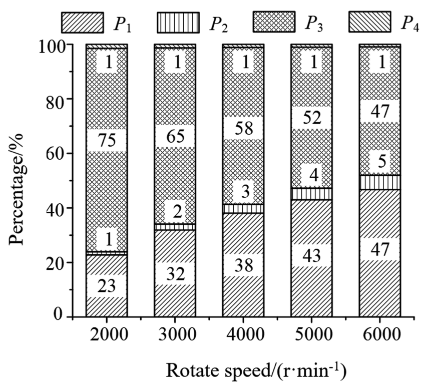

Fig. 5 Change rule of ratio of heat transfer rate with revolution speed

From Fig. 5, it can be seen that the percentage of bearing coil copper losses in the total heat source of the bearing decreases from 76% to 48%, while the percentage of eddy current losses in the total heat source of the bearing increases from 24% to 52%. This is because with the increase in rotor rotational speed, eddy current losses increase while copper losses stay constant, resulting in a greater proportion of eddy current losses relative to copper losses. Furthermore, due to the increased speed, the heat transfer rate at the rotor end face increases, resulting in a continuous increase in the heat transfer rate of eddy current losses to the atmosphere (P_2). The heat transferred to the atmosphere from the bearing increases from 2% to 6% of the total heat transferred to the atmosphere, and the heat transferred to the fluid decreases from 98% to 94%.

3.3 Relationship with inlet oil flow rate

Changes in flow rate significantly affect the flow velocity within the bearing, increasing flow velocity will accelerate bearing cooling, thereby affecting the heat dissipation pattern of the magnetic core. The results are shown in Table 5.

Table 5 Change rule of heat transfer rate of bearing with oil flow

Oil flow rate Q /(L · min^{-1})	Eddy current loss → fluid heat transfer rate P_1/W	Eddy current loss → atmospheric heat transfer rate P_2/W	Coil copper loss → fluid heat transfer rate P_3/W	Coil copper loss → atmospheric heat transfer rate P_4/W
0.02	24.88	1.26	81.36	1.62
0.03	24.88	1.06	81.50	1.49
0.04	25.08	0.95	81.54	1.43
0.05	25.19	0.87	81.59	1.38
0.06	25.27	0.81	81.63	1.35

From Table 5, it can be seen that as the inlet oil flow increases, the bearing eddy current losses and the heat transfer rate from the coil to the fluid gradually increase, while the heat transfer rate to the atmosphere gradually decreases. Moreover, the magnitude of the heat transfer rate change is relatively small. Therefore, it can be inferred that the effect of inlet oil flow on the heat dissipation pattern of the bearing is not significant. Further analysis on the proportion between P_1 and P_4 is presented in Fig. 6.

Building on the insights from Fig. 6, it can be observed that the increase in inlet oil flow does not affect the ratio of eddy current losses to coil copper losses. Coil copper losses account for 76% of the total heat source of the bearing, while eddy current losses account for 24% of the total heat source of the bearing. This is because the inlet oil flow does not have an impact on the bearing's heat source. As inferred from the proportion between P_1 and P_4, with the increase in inlet oil flow, there is no significant change in the proportion of heat transferred by the bearing to the atmosphere and the fluid. Therefore, it can be concluded that the magnetic pole inlet oil flow has almost no effect on the heat dissipation pattern of the bearing.

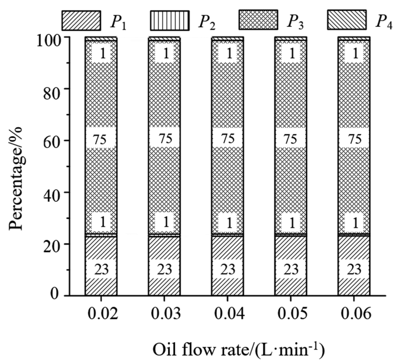

Fig. 6 Change rule of ratio of heat transfer rate with oil flow

4 Experiment

The test conditions for the magnetic fluid bearing test stand are as follows: the input current can be adjusted within the range of 2 A to 3 A, and the rotational speed can be adjusted within the range of 50 r · min^{-1} to 500 r · min^{-1}. There is a JCJ100TTP temperature sensor attached to the stator of the bearing, with a maximum temperature measurement range of − 55.0 ℃ to + 125.0 ℃ and an accuracy of ±0.5 ℃, as shown in Fig. 7. The signals are connected to the DH5922D dynamic signal testing and analysis system.

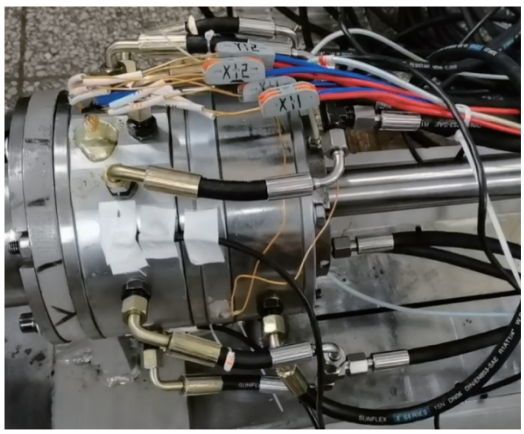

Fig. 7 Pasting temperature sensor

Because the oil tank has a relatively large volume, the inlet oil temperature can be considered constant and at room temperature. The temperature at the outlet is measured using a temperature sensor under different input currents. The temperature difference between the outlet and the oil tank temperature is then calculated, giving the temperature difference between the inlet and outlet under different input currents. The temperature difference curves between the inlet and outlet obtained from experiments and simulated calculations are shown in Fig. 8.

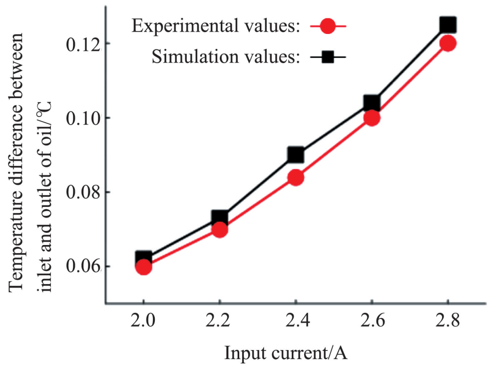

Fig. 8 Simulation and measure values of temperature difference between inlet and outlet under different input current

According to Fig. 8, it can be observed that the temperature difference between the inlet and outlet of the bearing in simulations exhibits a linear increasing trend with the increase in input current. As the current increases from 2.0 A to 2.8 A, the temperature difference between the inlet and outlet increases linearly from 0.06 ℃ to 0.12 ℃. There is some deviation between the actual measured values and the simulated results, with a maximum error of 6.7%. However, the trend of the temperature difference between the inlet and outlet matches the simulated values, and the error falls within an acceptable range.

Temperatures at the oil outlet under different speeds are measured using a temperature sensor. Subtracting the temperature of the oil in the tank from the measured temperatures at the oil outlet gives the temperature difference between the oil inlet and outlet under different speeds. Fig. 9 shows the temperature difference curve obtained from experiments and simulation calculations for the oil inlet and outlet.

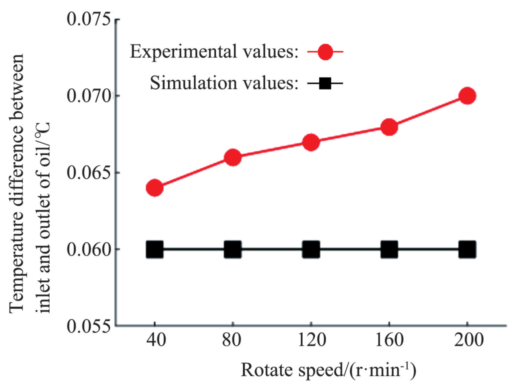

Fig. 9 Simulation and measure values of temperature difference between inlet and outlet under different rotate speed

According to Fig. 9, it can be observed that the temperature difference between simulated inlet and outlet of the bearing remains relatively constant as the speed increases. As the speed increases from 40 $r \cdot min^{-1}$ to 200 $r \cdot min^{-1}$, the temperature difference between the inlet and outlet consistently stays at 0.060 ℃. In contrast, during experiments, the temperature difference between the inlet and outlet increases from 0.064 ℃ to 0.070 ℃ as the speed increases, although the change is not very significant. This is because in the simulation, the inlet oil temperature is theoretically kept constant and does not account for the heat generation of the oil pump motor. In actual experiments, the heat generated by the oil pump motor causes an increase in the oil temperature. The trend in temperature differences between the inlet and outlet from experiments generally matches the simulated baseline, with a maximum error of 14.3%. The experimental process is influenced by various factors, resulting in a certain deviation between the measured temperature values and the simulated ones. However, the temperature change trend remains basically the same.

5 Conclusion

(1) By extracting the heat transfer rates between the various coupled heat exchange surfaces, the overall heat dissipation characteristics of the bearing are analyzed. This is done to investigate the cooling efficiency of the oil and study the impact of parameter variations on the overall heat dissipation of the bearing. The results indicate that increasing the inlet oil flow rate is beneficial for enhancing the cooling efficiency.

(2) The dissipation patterns of the two major heat sources and their interactions with parameters are revealed. The results indicate that oil is the primary cooling pathway for the bearing, and the cooling efficiency of the oil can reach 98.84%.

(3) The accuracy of the multi-field coupling theory in calculating temperature rise is verified. The results show that gradually increasing the input current results in a linear increase in the stator's average temperature, with a maximum error of 4.50% between measured and simulated values. Similarly, the temperature difference between the inlet and outlet of the oil linearly increases, with a maximum error of 6.70%. As the rotational speed is gradually increased, the trend in stator temperature changes is largely consistent, with a maximum error of 5.36%. However, the maximum error in the temperature difference between the inlet and outlet of the oil is 14.30%.

References

[1] DENG X L, DAI W K, ZHOU L F, et al. Thermal characteristics analysis and test of spindle-column system for

CNC machine tool[J]. Optics and Precision Engineering, 2020, 28(3):601-609. (In Chinese)

[2] LI M Y, CHEN J M, HU Q. Thermal performance analysis of conical hydrostatic bearing based on conjugate heat transfer method[J]. Mechanical Research and Application, 2014, 27(3):36-38, 49. (In Chinese)

[3] SHI X, KANG Y, FAN L, et al. Thermo-structural coupling calculation method for permanent magnetic synchronous motorized spindle[J]. Journal of Huazhong University of Science and Technology (Natural Science Edition), 2017, 45(2):50-54, 60. (In Chinese)

[4] YIN C, ZHANG L, WANG B, et al. Multi-physical field coupling simulation and experimental study on thermal characteristics of hydrostatic spindle[J]. Lubrication Engineering, 2019, 44(9):126-135. (In Chinese)

[5] HOLKUP T, CAO H, KOLÁR P, et al. Thermo-mechanical model of spindles[J]. Cirp Annals-Manufacturing Technology, 2010, 59(1):365-368.

[6] SHENOY S B, PAI R S, RAO D S, et al. Elasto-hydrodynamic lubrication analysis of full 360'journal bearing using CFD and FSI techniques[J]. World Journal of Modelling and Simulation, 2009, 5(4): 315-320.

[7] LIU H, XU H, ELLISON P J, et al. Application of computational fluid dynamics and fluid-structure interaction method to the lubrication study of a rotor-bearing system [J]. Tribology Letters, 2010, 38: 325-336.

[8] WENG G, TIAN X, ZHAO J, et al. Determinate mathematical model of couple bearing force of magnetic-liquid suspension guide-way with complicate constraint [J]. High Technology Letters, 2018, 24(4):440-448.

[9] CHEN X, JIAO Q, TAN X, et al. Numerical simulation of ultrasonic enhancement by acoustic streaming and thermal effect on mass transfer through a new computation model[J]. International Journal of Heat and Mass Transfer, 2021, 171: 121074.

[10] ZHOU D, LU Z, GUO T, et al. A loosely-coupled gas-kinetic BGK scheme for conjugate heat transfer in hypersonic flows[J]. International Journal of Heat and Mass Transfer, 2020, 147: 119016.

[11] SUN Q, YUAN H, ZHOU H. Preliminary study on electromagnetic thermal coupling numerical simulation technology of static inductor[C]//Journal of Physics: Conference Series. Ottawa, Canada: IOP Publishing, 2021: 1-9.

[12] JIANG W, JAHNS T M. Coupled electromagnetic-thermal analysis of electric machines including transient operation based on finite-element techniques[J]. IEEE Transactions on Industry Applications, 2014, 51(2): 1880-1889.

[13] REN Z, LI N. Structural design and experimental study of radial electromagnetic bearings with large supporting force[J]. Bearing, 2018 (4):39-44. (In Chinese)

[14] ZHAO J, WANG X, LIU H, et al. Analysis of fluid vibration transfer path and parameter sensitivity of swash plate axial piston pump[J]. High Technology Letters, 2022, 28(2):217-226.

[15] ZHAO C, MA P, GONG C, et al. Research on characteristics of the high precision hydrostatic spindle system base on one-way fluid-solid interaction[J]. Lubrication Engineering, 2014, 39(5):62-68. (In Chinese)

CHEN Liwen, born in 1978. He received his Ph. D degree in fluid transmission and control from Yanshan University in 2023. He also obtained M. S. degree from Inner Mongolia University of Technology in 2006. His research directions include hydraulic equipment design, flow field simulation calculation, and intelligent rehabilitation mechanism design.